



**HAL**  
open science

## Inorganic-organic hybrid pigments based on carminic acid and clay minerals

Graycyellê R.S. Cavalcanti, Francisco Rodrigues, Guanzheng Zhuang, Sebastien Balme, Jean-Marc Janot, Maria G Fonseca, Maguy Jaber

► **To cite this version:**

Graycyellê R.S. Cavalcanti, Francisco Rodrigues, Guanzheng Zhuang, Sebastien Balme, Jean-Marc Janot, et al.. Inorganic-organic hybrid pigments based on carminic acid and clay minerals. *Dyes and Pigments*, 2021, 190, pp.109306. 10.1016/j.dyepig.2021.109306 . hal-03236376

**HAL Id: hal-03236376**

**<https://hal.sorbonne-universite.fr/hal-03236376>**

Submitted on 26 May 2021

**HAL** is a multi-disciplinary open access archive for the deposit and dissemination of scientific research documents, whether they are published or not. The documents may come from teaching and research institutions in France or abroad, or from public or private research centers.

L'archive ouverte pluridisciplinaire **HAL**, est destinée au dépôt et à la diffusion de documents scientifiques de niveau recherche, publiés ou non, émanant des établissements d'enseignement et de recherche français ou étrangers, des laboratoires publics ou privés.



26 **Abstract**

27

28 Hybrid pigments based on carminic acid (CA) stabilized by clay minerals have been prepared.  
29 Three different pathways were used: CA@saponite; CA@Al-pillared saponite; and hydrogels  
30 of saponite-CA or montmorillonite-CA covered by polyorganosilane (POS). Pigments were  
31 characterized by a set of different techniques including X-Ray diffraction (XRD),  
32 transmission electron microscopy (TEM), infrared spectroscopy (FTIR), solid state nuclear  
33 magnetic resonance (NMR) and time-resolved fluorescence (TRF) spectroscopies. The color  
34 parameters, i.e.,  $L^*a^*b^*$ , were measured. In addition, the photostability of the samples under  
35 visible light was evaluated. The results showed that CA@PilSap presented a greater stability  
36 compared to CA@Saponite. The pigments obtained from hydrogels presented the greatest  
37 light stability due to the coverage with POS that acts as a protective layer.

38

39 **Keywords:** hybrid pigments; saponite; carminic acid; photodegradation

40

41

42

43

44

45

46

47

48

49

50

## 51 **1. Introduction**

52 The use of pigments from natural origins has been reported since ancient times for various  
53 purposes such as paints, cosmetics, dyeing textiles and coloring foods [1,2]. Dyes derived  
54 from *coccid* insects are commonly used and constitute one of the most known and exploited  
55 classes of red organic dyes at the present day [3].

56 Carminic acid (CA), (IUPAC nomenclature 17-C- $\alpha$ -glucopyranosyl-3,5,6,8-tetrahydroxy-1-  
57 methyl-2-anthraquinone), has been reported as the main derivative dye from cochineal with a  
58 high yield of extraction [2–4]. CA is vulnerable to thermal variations and photodegradation  
59 when used in its pure form. This phenomenon is commonly observed in paintings and  
60 promotes the increase of studies related to both the photodegradation mechanisms and the  
61 development of new stable pigments derived from CA [5,6].

62 The increase in system stability has been innumerable times related to the preparation of  
63 pigments involving inorganic matrices. Studies have shown that the synergy of organic and  
64 inorganic compounds in hybrid materials may form new materials with enhanced properties  
65 [4,7-9]. In the case of pigments, greater stability can be improved by the formation of organic-  
66 inorganic hybrid pigments.

67 The development of pigments based on inorganic substrates and organic compounds, is not a  
68 recent issue. Maya blue, composed of palygorskite and indigo dye, is a famous archeological  
69 example of organic-inorganic hybrid pigment. It was widely used in paintings, murals and  
70 ceramics from the Mayan civilization [7,8]. Its incredible stability against acid, alkaline and  
71 organic corrosion and degradation over time has recently attracted much interest in the fields  
72 of materials, chemistry and archeology [4,9].

73 Although the real nature of Maya blue is controversial, it is believed that the unique clay-dye  
74 interaction between palygorskite and indigo endows its remarkable stability. Maya blue  
75 encourages that clay-dye hybrid pigments may be a promising way to develop new durable

76 hybrid pigments. In general, clay minerals have specific physicochemical properties such as  
77 adsorption, cation exchange capacity, swelling capacity, ability to form colloidal solutions,  
78 optimum rheological behavior and dispersibility in water; which have allowed them to be  
79 used in different ways in various applications [10,11]. In addition, studies with other clay  
80 minerals allow research about the impact of the structure and layer loading on the  
81 coordination of metallic ions, as well as the capacity of interactions with positively charged  
82 species such as cationic dyes [12,13].

83 Recently, other clay minerals have been used as an inorganic matrix to prepare hybrid  
84 pigments such as saponite [14,15], montmorillonite [6,16], palygorskite [8,17], sepiolite  
85 [7,18] and halloysite [19], etc. Montmorillonite (Mt) and saponite (Sap) are phyllosilicates  
86 belonging to the smectite group. The structural variability, as well as the possibility of  
87 modifying the clay minerals belonging to this group, allows different interactions with dyes  
88 that vary according to the structural composition [19, 20].

89 The interaction of dye molecules with clay minerals is the key parameter to prepare inorganic-  
90 organic hybrid solids that are more stable than the dyes in their isolated form [11,22].

91 Although they are excellent adsorbents for different organic molecules, clay minerals present  
92 limitations in relation to the species that can be adsorbed. Therefore, some modifications have  
93 been proposed to overcome these limitations [23,24]. The main clay modifications reported in  
94 the literature are ion exchange [25], intercalation of cationic surfactants [26], pillaring with  
95 different metal oxides [27], silylation [28], coating of hexadecyltrimethoxysilane (HDTMS)  
96 and tetraethoxysilane (TEOS) [29].

97 In this context, the present work intended to synthesize new stable pigments based on CA and  
98 clay minerals. Three different pathways were used: direct adsorption of CA on raw synthetic  
99 saponite; adsorption of CA on Al-pillared saponite; and hydrothermal treatment of CA with  
100 hydrogels of saponite and montmorillonite followed by covering with polyorganosilane

101 (POS). The prepared pigments were characterized, and their chemical and light stabilities  
102 were evaluated.

## 103 **2. Experimental**

104 All chemicals were analytical grade and were used without additional purification. In Table  
105 SM1 are summarized the list of samples and methods used in the synthesis.

106

### 107 *2.1 Synthesis of saponite (Sap)*

108 Synthetic saponite was prepared from the reagent mixture, added in the following order:  
109 deionized water (65.38 g, 3.63 mol), hydrofluoric acid (0.38 g, 0.95 mmol, 40% w/w; Fluka),  
110 sodium acetate (0.18 g, 2.15 mmol, 99%; Sigma-Aldrich), magnesium acetate (3.46 g, 16.2  
111 mmol, 99%, Sigma-Aldrich), alumina (0.34 g, 3.33 mmol, 99.8%; Sigma-Aldrich) and silica  
112 (1.15 g, 19.14 mmol, Aerosil 380; 99.8%; DEGU). The hydrogels were prepared with the mol  
113 composition of  $\text{Na}_{0.4}[(\text{Si}_{3.6}\text{Al}_{0.3})\text{Mg}_3\text{O}_{10}(\text{OH},\text{F})_2]$ , aged for 4 h at room temperature under  
114 magnetic stirring and then was autoclaved at 220 °C for 72 h. The autoclaves were cooled to  
115 room temperature and the product were washed with deionized water and centrifuged for 7 to  
116 10 times [30].

### 117 *2.2 Pillaring process of saponite (PilSap)*

118 The preparation of Al-pillared saponite followed the procedure adapted from Bergaoui *et al.*  
119 (1995) [31]. First, the pillaring agent was obtained by hydrolysis of aluminum chloride (1.6 g,  
120 12 mmol Al 99%; Sigma-Aldrich) with a NaOH (1.01 g, 26.4 mmol OH, 98.9%; Merck)  
121 solution up to 2.2 OH:Al ratio and final concentration of 0.1 mol L<sup>-1</sup>. The reactional mixture  
122 was aged for 24 h at room temperature (~25 °C) under magnetic stirring. Meanwhile, the  
123 suspension (7.5 mmol Al<sup>3+</sup> g<sup>-1</sup> clay) containing saponite (1.6 g) was prepared by suspending  
124 the clay in water (500 mL) and aged for 3 h at the same conditions. Later, aluminum pillaring  
125 solution (120 mL) was added dropwise (~0.5 mL min<sup>-1</sup>) to a clay suspension and was

126 maintained under magnetic stirring for 24 h at room temperature. The obtained solid (Sap-Al)  
127 was centrifuged at 8000 rpm for 20 min and washed with deionized water and dried at 50 °C  
128 for 24 h. After that, sample was calcined up to 500 °C for 2 h and then denoted PilSap.

129

### 130 *2.3 Preparation of hybrid pigments*

131

#### 132 *2.3.1 Adsorption procedure*

133

134 Saponite and Al-pillared saponite samples were loaded with carminic acid (CA; 99%; Sigma-  
135 Aldrich, pKa values of 2.8, 5.4 and 8.1): for each sample, a clay amount (300 mg) was  
136 suspended in an aqueous solution of carminic acid (100 mL, 0.6 g L<sup>-1</sup>) and was left under  
137 stirring for 4 h at room temperature (~25 °C) under magnetic stirring. The pH of the solution  
138 was adjusted to 2.5, which is the pH where CA species are neutral. The samples were then  
139 centrifuged, washed with deionized water and dried at 50 °C for 24 h, following the same  
140 method previously described [6].

141

#### 142 *2.3.2 Pigments synthesis from clay hydrogels*

143

144 The hydrogels were prepared with the mol composition of Na<sub>0.4</sub>[(Si<sub>3.6</sub>Al<sub>0.3</sub>) Mg<sub>3</sub>O<sub>10</sub>(OH,F)<sub>2</sub>]  
145 and Na<sub>0.4</sub>[(Si<sub>4</sub>)(Al<sub>1.6</sub>Mg<sub>0.4</sub>)O<sub>10</sub>(OH,F)<sub>2</sub>], for saponite and montmorillonite precursors,  
146 respectively. The amounts of used salts are described in the Table SM2. The mixtures were  
147 maintained under stirring at room temperature for 48 h at pH 5. Then, the respective  
148 hydrogels (12 g) and carminic acid (1.2 g, 10% m/m) were autoclaved at 120 °C for 10 days.  
149 After that, the autoclaves were cooled to room temperature and the final product were washed  
150 with deionized water (~ 150 mL) and centrifuged and dried at 50 °C for 48 h. Saponite and

151 montmorillonite precursors samples obtained by coprecipitation were named CA-precSap-120  
152 and CA-precMt-120, respectively.

153

### 154 *2.3.3 Coating with TEOS / HDTMS*

155 Coating method followed methodology described by Zhuang *et al.* 2019 [19]. First, CA-  
156 precSap-120 or CA-precMt-120 (200 mg) was dispersed in ammonia (25%; Sigma-Aldrich)  
157 saturated in ethanol (95%; VWR) solution (10 mL) prepared in 9:1 volume/volume  
158 proportion. Suspension was maintained under magnetic stirring for 5 min. Then, TEOS (99%;  
159 Sigma-Aldrich) (0.32 mL, 0.15 mmol) and HDTMS (85%; Sigma-Aldrich) (0.546 mL, 0.15  
160 mmol) were added into the mixture that was ultrasonicated at 50 °C for 30 min. Finally,  
161 deionized water (1.44 mL) was quickly injected into the solution that was maintained under  
162 same conditions for 1 h. The samples after coating were denominated CA@Sap-Si, CA-  
163 precSap-120-Si and CA-precMt-120-Si.

164

### 165 *2.4 Desorption study*

166

167 Desorption experiments were performed by dispersing the pigments (10 mg) in deionized  
168 water (10 mL) under magnetic stirring at room temperature for 20 min. Then, the solids were  
169 centrifuged at 10.000 rpm for 5 min. Finally, the amount of dye remaining in the supernatant  
170 was determined by UV-Vis molecular absorption spectroscopy with an Ocean Optics device  
171 with halogen light source and deuterium HL-2000-FHSA operating in the 200-900 nm range.  
172 The supernatants were placed in quartz tubes with accessories for liquids containing 1 cm  
173 optical path. The concentration of carminic acid in solution was quantified at 485 nm in the



174 range of 2 to 50 mg L<sup>-1</sup> and the amount of dye ( $q_e$ ) in the supernatant after desorption was  
175 determined according to Equation 1

176

$$177 \quad q_e = \frac{(C_e)V}{m} \quad (1)$$

178

179 where  $C_e$  (mg L<sup>-1</sup>) are the concentrations of the dye after desorption,  $m$  (mg) mass of clay and  
180  $V$  (L) the volume of deionized water.

181

### 182 **3. Characterizations**

#### 183 *3.1 X-ray diffraction (XRD)*

184 X-ray diffractograms were recorded using the D8 Advance Bruker-AXS X-ray diffractometer  
185 with 30 kV voltage and 30 mA current and CuK $\alpha$  radiation ( $\lambda = 1.5405 \text{ \AA}$ ). The XRD patterns  
186 were obtained between ( $2\theta$ ) of 5 to 80 ° with a scan rate of 0.5 degrees min<sup>-1</sup>.

187 Sap, Sap-Al and PilSap samples required an additional procedure to obtain higher quality  
188 diffractograms. Thus, the solid (200 mg) was dispersed in water (2 mL) and was kept under  
189 magnetic stirring until a homogeneous dispersion. Subsequently the mixture was deposited  
190 onto a glass slide to form a homogeneous layer. The slices were dried at 50 °C for 24 h and  
191 resulted in a film formation. The diffractograms were then collected under the same  
192 conditions as for the other samples.

193

#### 194 *3.2 ATR-FTIR*

195 Infrared analyzes were performed on the Agilent Cary 630 FTIR spectrometer using the  
196 Attenuated Total Reflectance mode (ATR) with a diamond crystal detector and the spectral  
197 resolution of 2 cm<sup>-1</sup> and 30 accumulation scans. The spectra were collected by the Microlab  
198 FTIR Software (Agilent Technologies) between 4000 and 600 cm<sup>-1</sup>.

199 *3.3 Thermal analysis (TG/DTG)*

200 Thermogravimetric analyses were performed using a TA Instrument SDT Q600 analyzer with  
201 a heating rate of 5 °C min<sup>-1</sup> from 25 °C to 900 °C, under dry air flow of 10 mL min<sup>-1</sup> and  
202 using an alumina crucible.

203

204 *3.4 Solid state nuclear magnetic resonance (<sup>13</sup>C CP-MAS- and <sup>27</sup>Al MAS-NMR)*

205

206 The <sup>27</sup>Al NMR spectra were obtained on a Bruker Avance III spectrometer equipped with a 4  
207 mm HX MAS probe, operating at a frequency of 130.33 MHz. Al (NO<sub>3</sub>)<sub>3</sub> (0 ppm) was used as  
208 an external standard. <sup>13</sup>C spectra were obtained on a Bruker Avance 500 spectrometer  
209 operating at a frequency of 60.37 MHz. Cross-polarization of protons (CP-MAS) was applied  
210 with a contact time of 1 ms. The samples were rotated at the magic angle at a frequency of 10  
211 kHz. The pulse length of <sup>13</sup>C was 5 ms (close to  $\Pi/2$ ) and the recycling delay was 3 s.

212

213 *3.5 Transmission electron microscopy (TEM)*

214 Transmission electron microscopy analyzes were performed under a JEOL 2010 microscope  
215 operating at 200 kV LaB6. To prepare the sample a few milligrams of the sample are mixed in  
216 a Beem capsule with Agar 100 embedding resin. After polymerization at 60°C overnight, the  
217 blocks are cut using a microtome equipped with a diamond knife. The ultra-thin slices about  
218 50 nm, are recovered on copper grids and examined. The micrography were treated using  
219 Gatan Software.

220

221 *3.6 Contact angle analysis*

222 The evaluation of the hydrophobicity of the pigments was performed from the preparation of  
223 pellets of 5 mm diameter in which a drop of 10  $\mu$ l of water was added to calculate the angle

224 generated between the plane tangent to the surface of the material on which the drop was  
225 deposited [8,32]. Adobe Photoshop software was used for the treatment of images.

226

### 227 *3.7 Time-resolved fluorescence*

228 The fluorescence lifetimes were obtained by the time-correlated single-photon counting  
229 technique. The fluorescence decay of CA and CA loaded in different materials were directly  
230 performed on powder deposited on a cover slide. The excitation wavelength was achieved by  
231 using a SuperK Extrem high power white supercontinuum laser (NTK Photonics, model EXR-  
232 15) as a continuum pulsed source. The wavelength ( $\lambda=580$  nm) was selected by coupling to a  
233 monochromator (Jobin–Yvon H10). The repetition rate was set to 38.9 MHz; the excitation  
234 pulse duration on this device is around 6 ps (full-width-at-half-maximum, FWHM). The  
235 emission of fluorescence is collected using a parabolic mirror and detected, after passing  
236 through a polarizer oriented at the magic angle ( $54.73^\circ$ ) to polarization of excitation, through  
237 a double monochromator ( $\lambda=660$  nm) Jobin–Yvon DH10 on a hybrid PMT detector HPM-  
238 100-40 (Becker & Hickl). The instrumental response function of the equipment was measured  
239 by using a dilute suspension of polystyrene nanospheres in water (70 nm of diameter) as a  
240 scattering solution; it was typically about 130-160 ps FWHM. Decays were collected at a  
241 maximum count rate of 15 kHz into 4096 channels using an acquisition card SPC-730(Becker  
242 & Hickl). The time per channel was set around 6 ps ch<sup>-1</sup> in order to fit a full decay in the  
243 experimental time window. All decays were collected to have at least 1.5 and 10<sup>6</sup> counts in  
244 total. Decay analysis was performed using a Levenberg–Marquardt algorithm. The  
245 fluorescence decay and anisotropy function were analyzed as a sum of exponential as

$$246 \quad I(t) = \sum_{i=1}^n a_i e^{(-t/\tau_i)} \quad (2)$$

247

248 Where  $I(t)$  is the fluorescence intensity,  $a_i$  a pre-exponential factor,  $\tau_i$  the fluorescence  
249 lifetime, Fluorescence lifetimes were calculated from data collected at magic angle by  
250 iterative adjustment after convolution of a pump profile (scattered light). We assumed a  
251 Poisson distribution of counts in the calculation of the  $\chi^2$  criterion; residuals profiles and  
252 autocorrelation function as well as Durbin-Watson and skewness factor were used in order to  
253 estimate the quality of the adjustment. The number of exponentials used for the fit was  
254 increased until all the statistical criterions were improved.

255

### 256 *3.8 Light-induced aging and diffuse reflectance UV-Vis*

257

258 Light-induced tests were performed by exposure of the solid pigments face to white light  
259 irradiation for 354 h, using an LED lamp set to provide 66 Klx of illumination intensity.

260 Photostability were evaluated over time by means of spectrophotometric measurements in  
261 triplicate by using an Ocean Optics device with light source of halogen and deuterium HL-  
262 2000-FHSA and incident light beam, with acquisition from the Ocean detector Optics  
263 USB4000. For each acquisition, an average of 30 scans were used under a wavelength range  
264 of 400 to 950 nm. The CIELAB data were calculated according to the “Commission  
265 Internationale of l’Eclairage” (CIE). The  $L^*$ ,  $a^*$  and  $b^*$  coordinates were obtained for the  $\Delta E^*$   
266 determination, which refers to changes in the pigment color over time of exposure to light.  
267 The total color difference ( $\Delta E^*$ ) was obtained from Equation 3:

268

$$269 \quad \left( (a_{*i+j} - a_{*i})^2 + (b_{*i+j} - b_{*i})^2 + (L_{*i+j} - L_{*i})^2 \right)^{1/2} \quad (3)$$

270

271 where, i and j refer to the number of measurements taken over time.

272 The reflectance spectra before and after exposure to light were also recorded for the samples  
273 of the pigments under the same conditions as described previously.

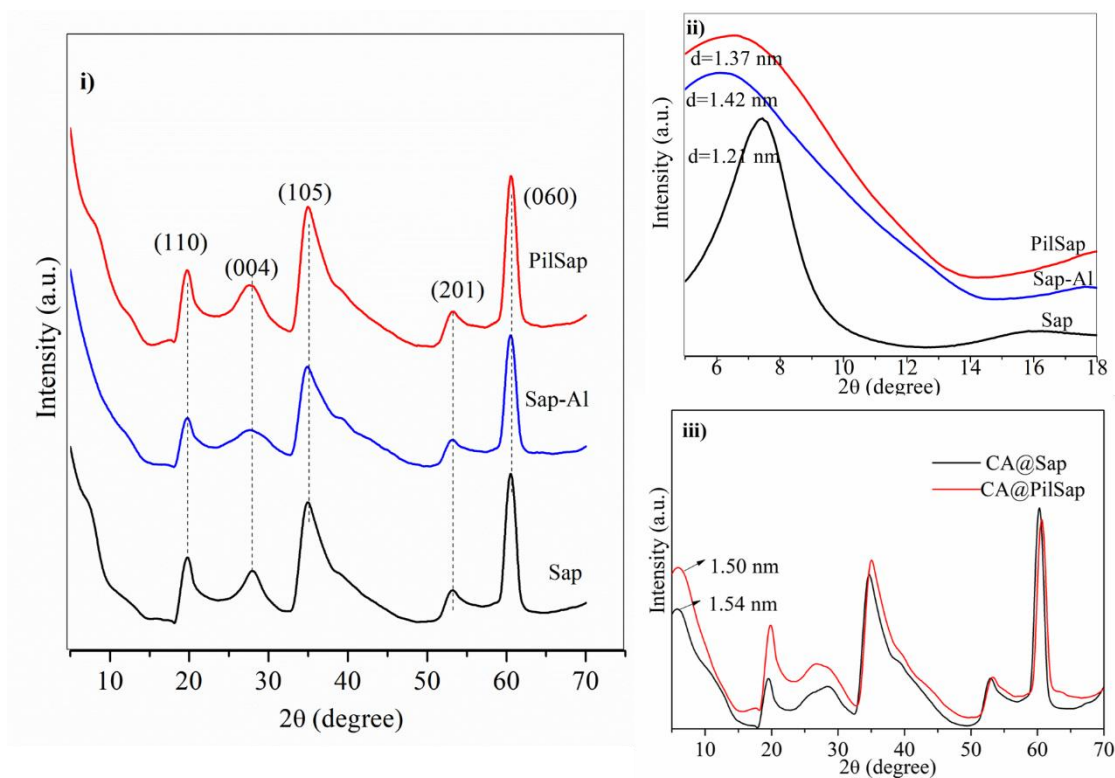
## 274 **4. Results and discussions**

### 275 *4.1 X-ray diffraction (XRD)*

276 XRD patterns for the saponite samples are presented in Figure 1i and showed the presence of  
277 characteristic clay mineral reflections. In particular, the reflection at  $60.6^\circ$  with a distance of  
278 0.153 nm (060) suggested the formation of a trioctahedral structure. Other reflections at  $19.7^\circ$ ,  
279  $27.8^\circ$ ,  $34.9^\circ$  and  $53.2^\circ$  are also characteristic of saponite [33,34]. For all samples the reflection  
280 in the 001 plane were enlarged or very weak, which is associated with the loss of periodicity  
281 along direction c and indicates disordered lamellar stacking [35]. Therefore, at low angles  
282 (Figure 1ii), oriented films were prepared as described in the experimental section and allow a  
283 better visualization of the (001) reflection of the saponite at  $2\theta = 7.34$  with a  $d_{001}$  value = 1.21  
284 nm, [36]. Therefore, basal spacing increased to 1.42 and 1.37 nm for Sap-Al and PilSap  
285 samples and suggested the intercalation of Keggin ion and the pillarization of the saponite  
286 after calcination [23,31,32].

287 After interaction with carminic acid (Figure 1iii), the (001) reflection plane presented a better  
288 definition. The increase in the basal spacing value from 1.21 to 1.54 nm in CA@Sap and from  
289 1.37 to 1.5 nm in CA@PilSap also suggested the intercalation of the dye in the interlayer  
290 space of the saponite.

291 Concerning the XRD patterns of the dried samples obtained from hydrogels, any reflection of  
292 the saponite and montmorillonite was not observed (see Figure SM1).



293

294 Figure 1 - X-ray diffractograms of (i) saponite and modified saponite before dye adsorption  
 295 between 8 and 70 ° ( $2\theta$ ) ii) saponite and modified saponite before dye adsorption between 2  
 296 and 20 ° ( $2\theta$ ) and iii) CA@Sap and CA@PilSap hybrids.

297

#### 298 4.2 Infrared Spectroscopy (ATR-FTIR)

299

300 Infrared spectroscopy was performed on samples before and after adsorption of carminic acid,  
 301 aiming to identify the presence of the CA in the samples and the nature of the dye/clay  
 302 minerals interactions. The structure and spectrum of carminic acid are presented in Figure 2i-  
 303 iii. The band at  $1710\text{ cm}^{-1}$  was assigned to C=O stretching of the carboxylic acid present in  
 304 the molecule [39]. The bands observed at  $1611$ ,  $1566$ , and  $1426\text{ cm}^{-1}$  were attributed to  
 305 quinone C=O stretching vibrations; C=C stretching and OH deformation, respectively [40].

306 For saponite and pillared saponite, characteristic bands of the clay mineral were observed:  
307 band around  $3684\text{ cm}^{-1}$  corresponds to the structural -OH stretching and the wide band around  
308  $982\text{ cm}^{-1}$  is attributed to the Si-O-Si stretching of the saponite structure [41].

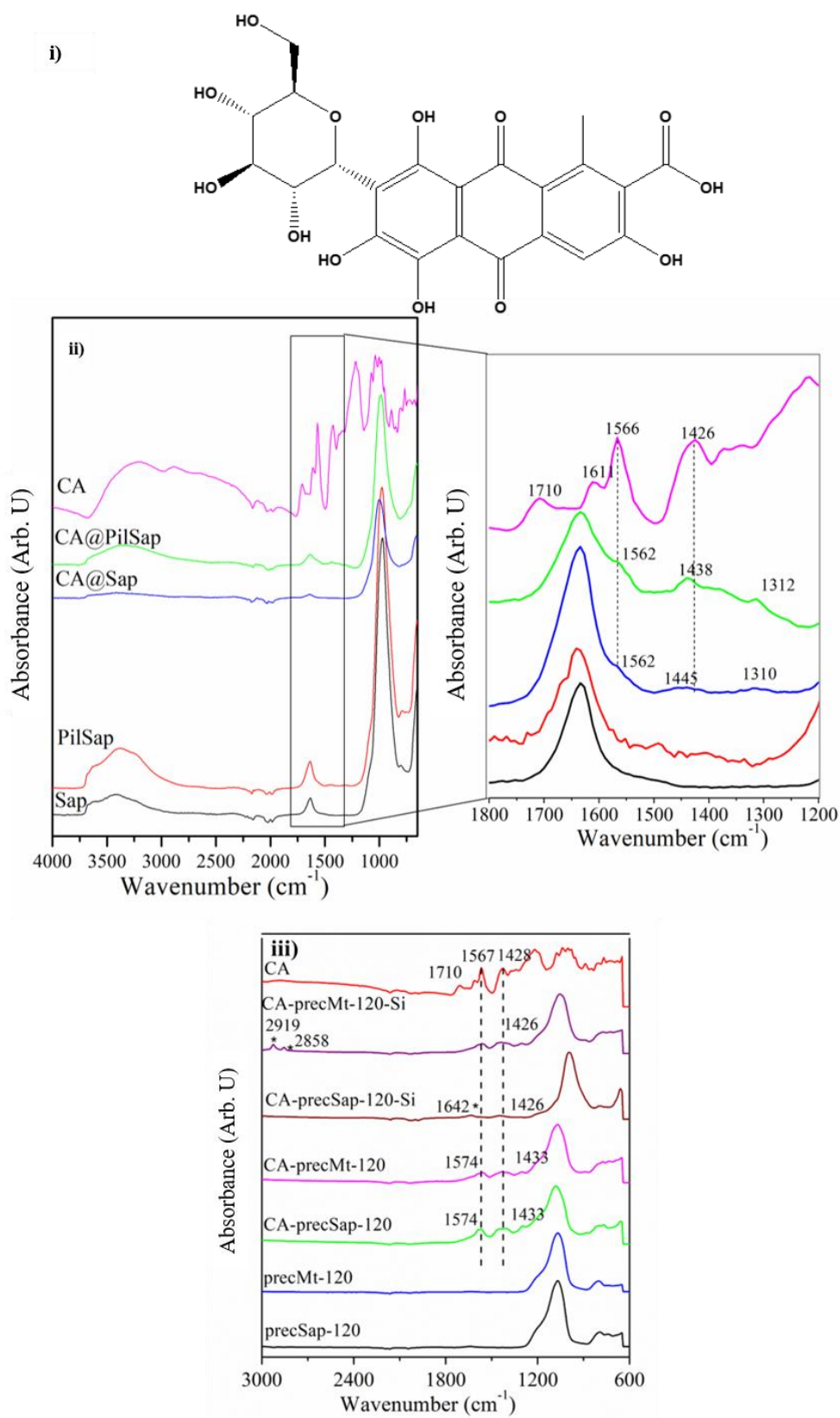
309 After CA sorption on Sap and PilSap, C=O stretching was not observed, suggesting that the  
310 interaction between the dye and the inorganic part occurred mainly via this function [39].  
311 C=C stretching did not show significant variation and is observed at  $1562\text{ cm}^{-1}$  for both clay  
312 samples. In contrast, the OH deformation shifted from  $1426$  to  $1445\text{ cm}^{-1}$  in CA@Sap and to  
313  $1438\text{ cm}^{-1}$  in CA@PilSap. This can also be due to an interaction between the catechol groups  
314 of the dye and the clay mineral.

315 In the samples heated at  $120\text{ }^{\circ}\text{C}$  without carminic acid, the spectra did not present  
316 characteristic bands of the clay mineral structure. However, the band around  $982\text{ cm}^{-1}$  can be  
317 assigned to the Si-OH stretching and formation of silicate in the clay hydrogels. (Figure 2iii).  
318 This may also indicate a poor crystallization of the saponite and montmorillonite precursors,  
319 which is in agreement with the XRD results [42].

320 Regarding samples obtained in the presence of CA and heated at  $120^{\circ}\text{C}$ , the presence of bands  
321 assigned to C=C stretching at  $1567\text{ cm}^{-1}$  and OH deformation at  $1419\text{ cm}^{-1}$  in both materials  
322 were associated to the anthraquinone functions that shifted compared to the one in the free  
323 carminic acid. This is due to the interaction between the dye and the oxide mixture present in  
324 the gels and suggests coordination between quinone and metal cations in the mixture, as well  
325 as the sorption of carminic acid on the oxide surface.

326 For both CA coated samples, the same bands than in the spectra of the uncoated solids were  
327 observed. However, the band at  $1426\text{ cm}^{-1}$  which is attributed to the -OH stretching in the  
328 anthraquinone appeared unchanged, which may be related to the migration of the dye  
329 molecules to the surface of the solids. The coating of the CA-precMt-120-Si was evidenced  
330 by the presence of the bands at  $2910\text{ cm}^{-1}$  and  $2858\text{ cm}^{-1}$  assigned to asymmetric and

331 symmetric CH stretchings and the band at  $1642\text{ cm}^{-1}$  for CA-precSap-120-Si assigned to  
 332 hexadecyl group [43].



333



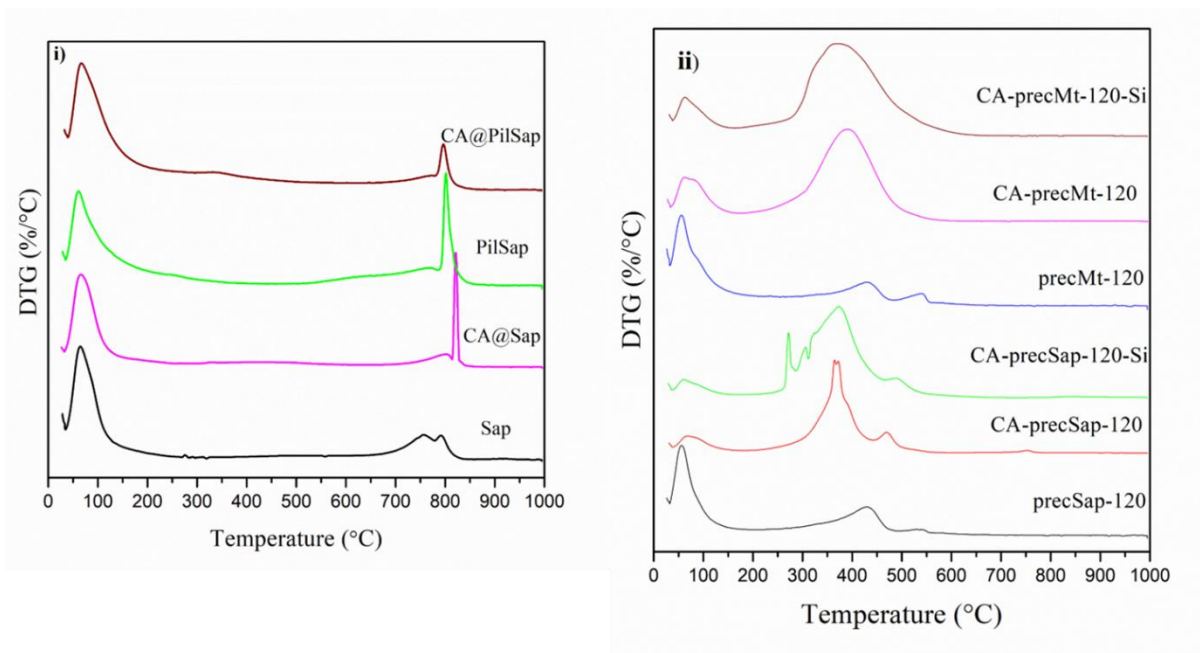
334 Figure 2 – i) Structure of the carminic acid and infrared spectra of ii) initial samples and  
335 hybrid pigments and iii) initial samples and hybrid pigments obtained by coprecipitation. (\*)  
336 TEOS/HDTMS signals.

337

#### 338 *4.3 Thermogravimetric analysis (TGA)*

339

340 TG (Figure SM2) and DTG (Figure 3i) curves for Sap and PilSap presented two mass loss  
341 steps. The first step was attributed to the adsorbed and interlayer water losses at  $T_{\max} = 65\text{ }^{\circ}\text{C}$   
342 and represented 8.6% for Sap and 5.4% for PilSap. The second event around 680-850  $^{\circ}\text{C}$  was  
343 attributed to the dehydroxylation of OH groups presented at the edges of the clay mineral  
344 layers and corresponded to 3.1% and 2.9% for pillared saponite and saponite, respectively.  
345 [44]. Free dye begins its degradation at 162  $^{\circ}\text{C}$  (Figure SM2). Samples CA@Sap and  
346 CA@PilSap loaded with carminic acid, presented two events of mass loss. Organic matter  
347 decomposition and dehydration occurred simultaneously in 32-164  $^{\circ}\text{C}$  and 35-200  $^{\circ}\text{C}$  and was  
348 associated to mass loss of 13.2% and 11.9% for CA@Sap and CA@PilSap, respectively. The  
349 last event between 700-800  $^{\circ}\text{C}$  referred to the clay mineral dehydroxylation for both samples.  
350 These results suggested that CA adsorbed in Al-pillaring clay presented higher thermal  
351 stability than free CA [6,16].



352

353 Figure 3 - DTG curves for i) references samples and hybrid pigments obtained by adsorption  
 354 ii) references samples and hybrid pigments obtained by coprecipitation.

355

356 The DTG curves of precMt-120, CA-Mt-120 and CA-precMt-120-Si (Figure 3ii) presented  
 357 two mass loss steps: the first one at about 40-160 °C with mass losses of 4.87%, 10.12% and  
 358 6.82% were attributed to dehydration (loss of physisorbed water). DTG curves of precSap-  
 359 120, CA-precSap-120 and CA-precSap-120-Si presented three distinct profiles with mass loss  
 360 in two, three and four events, respectively. The higher mass loss (48%) obtained at 280 °C  
 361 indicated that the dye degraded at higher temperatures compared to its isolated form (162°C)  
 362 due probably to a strong interaction with the inorganic matrix [45].

363

#### 364 4.4 $^{27}\text{Al}$ and $^{13}\text{C}$ CP MAS solid state nuclear magnetic resonance

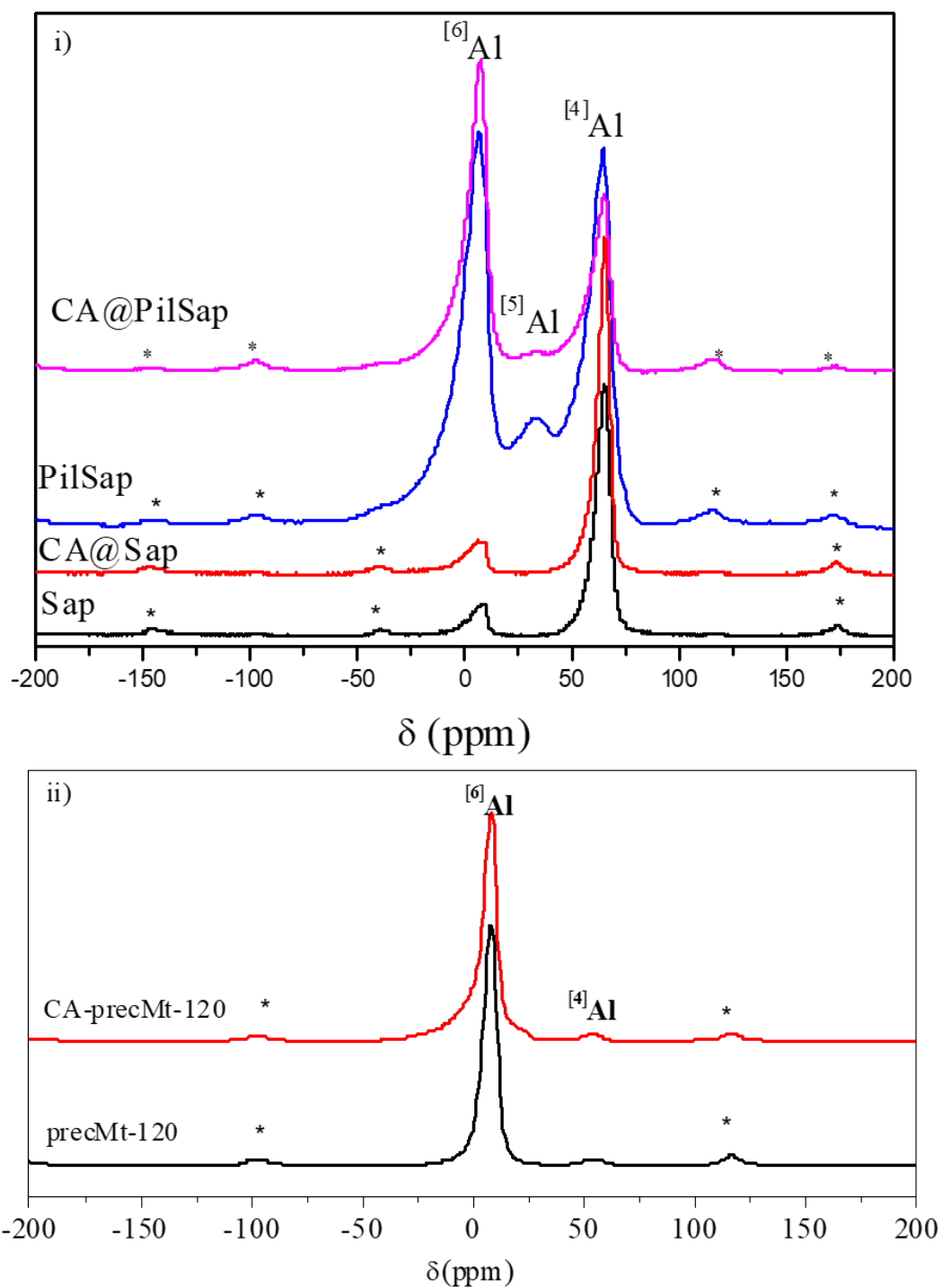
365

366 The  $^{27}\text{Al}$  NMR spectra for the Sap and PilSap samples are shown in Figure 4i-ii. Both samples  
 367 presented signals at 65.6 ppm due to the presence of structural tetrahedral aluminium  
 368 [27,46,47]. However, PilSap exhibited two new signals at 6.37 and 33.4 ppm, that were

369 attributed to hexa- and penta-coordinated Al, respectively. The high intensity signal refers to  
370 hexacoordinated aluminium ( $^{VI}Al$ ) in the pillars. The tetraordinated aluminium ( $^{IV}Al$ )  
371 signals refer to a central overlap aluminium in the Keggin structure that comprises of 13 Al  
372 atoms with a tetrahedral Al-center atom surrounded by 12 octahedral Al atoms [48,49]. The  
373 obtained data suggested the successful formation of the aluminium pillars in the PilSap  
374 sample.

375  $^{27}Al$  NMR spectra obtained for CA@Sap presented a similar profile to the one observed in  
376 Sap. Moreover, chemical shifts changed from 8.41 to 6.97 ppm in the signal attributed to  
377  $^{VI}Al$ . This shift may suggest the interactions between CA and Si-OH-Al-OH in the Sap [6,16].  
378 In contrast, the CA@PilSap spectrum showed a significant decrease in peak intensity at 33.4  
379 ppm for penta-coordinated aluminium and was related to an interaction between the  
380 aluminium and the dye.

381 Hydrothermally treated samples exhibited similar  $^{27}Al$  NMR spectra with an intense peak  
382 centered at 7.83 ppm attributed for hexacoordinated aluminium ( $^{VI}Al$ ) and a signal at 54 ppm  
383 attributed to tetraordinated aluminium ( $^{IV}Al$ ) [50,51].



384

385 Figure 4-  $^{27}\text{Al}$  NMR spectra of (i) precursor matrix and hybrid pigments obtained by  
 386 adsorption, and ii) precursor matrix and hybrid pigment obtained by coprecipitation, (\*) Side  
 387 spinning bands.

388

389  $^{13}\text{C}$  CP/MAS NMR spectra of carminic acid and the derived pigments are shown in Figure 5i-  
390 ii and the chemical shifts are also summarized in Table 1. Resonance spectral regions for  
391 anthraquinone structure were observed as described in the literature [6,16]. The 60-80 ppm  
392 region refers to the sugar moiety present in the molecule, while the 20.6 ppm peak is  
393 attributed to the methyl group on C-8. The signals at 185 and 171 ppm are related to the  
394 ketones and carboxylate functions, respectively. The spectrum of CA@Sap presented a  
395 similar profile to the one observed for the free dye, but some displacements were noted from  
396 119 ppm to 113 ppm, from 112 ppm to 102 ppm and from 105 ppm to 100 ppm, attributed to  
397 C-2, C-4a,5 and C-8 atoms, respectively [4]. The shifts can be correlated to both the  
398 protection effect and the inductive effect through the carbon environments in the  
399 anthraquinone part of the dye after interaction between the OH groups of the C-2 and C-4  
400 atoms with saponite. However, the region in the spectrum assigned to C-4 as well as C-1 and  
401 C-3 carbons are not well resolved to observe the chemical shifts.

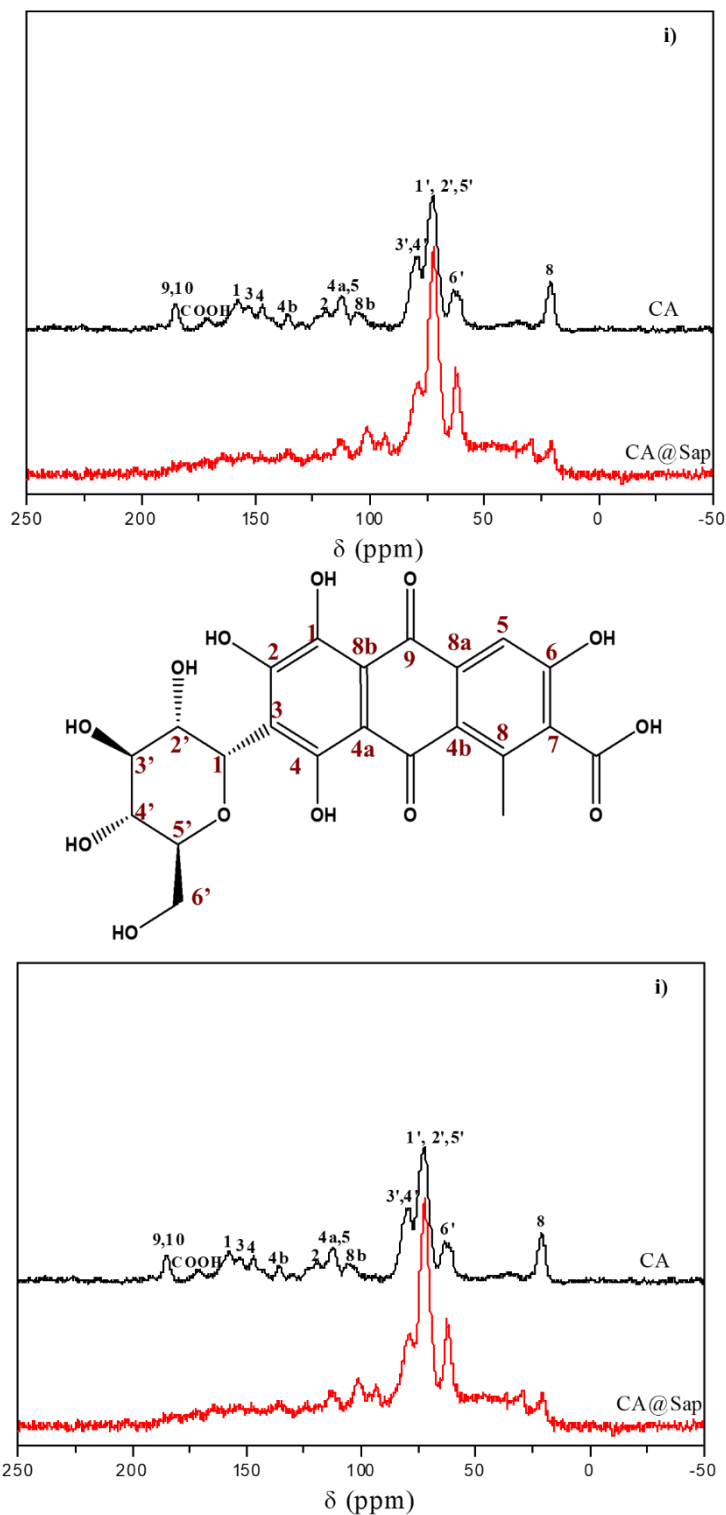
402 Figure 5ii showed  $^{13}\text{C}$  CP/MAS NMR spectrum for CA-precMt-120-Si. Variations in the  
403 chemical shifts were also observed, from 119 ppm to 124 ppm, from 153 ppm to 149 ppm and  
404 from 20.6 ppm to 22.9 ppm, attributed to C-2, C-3 and C8 atoms, respectively. In the region  
405 of the C-9,10, the signal was changed from 185 to 182 ppm for CA-precMt-120, which  
406 suggests the chelation of the anthraquinone dye with the aluminum oxide dispersed in the gel.  
407 Similar results were obtained in previous work [4,6,16].

408 Table 1 - Main chemical shifts observed in the  $^{13}\text{C}$  CP/MAS NMR spectra for the CA@Sap  
409 and CA-precMt-120 samples.

<b>Carbon</b>	<b><i>Chemical shifts (ppm)</i></b>		
	CA	CA@Sap	CA-precMt-120
<b>C-2</b>	119	113	124
<b>C-3</b>	153	-	149
<b>C-4a,5</b>	112	102	-
<b>C-8b</b>	105	100	-
<b>C-8</b>	20.6	20.6	22.9
<b>C-9,10</b>	185	-	182

410

411



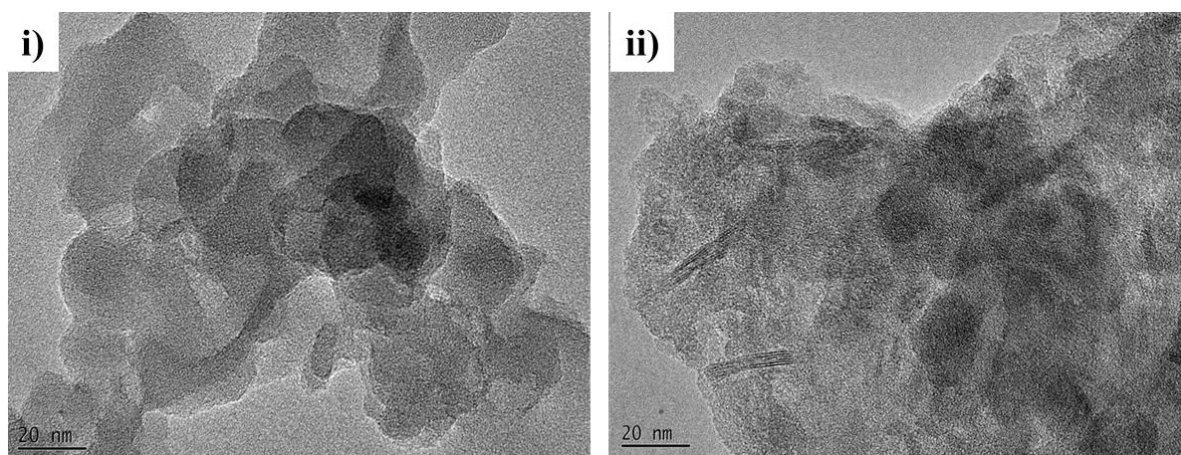
412

413 Figure 5-  $^{13}\text{C}$  CP/MAS NMR spectra for carminic acid and i) pigments obtained by  
 414 adsorption, and ii) pigment obtained by coprecipitation.

415

416 *4.5 Transmission electron microscopy (TEM)*

417 TEM micrographs (Figure 6) indicated that after hydrothermal synthesis, the samples did not  
418 present profiles characteristic of the smectites, which is in agreement with XRD analysis, that  
419 suggests the formation of solids with low crystallinity. Moreover, the CA-precMt-120 sample  
420 (Figure 6ii) presented layered structures in the gel but not uniform distribution. Presence of  
421 layered structures can promote additional stability to the pigment compared to CA-precSap-  
422 120 sample. The synthesis was performed at neutral pH and relatively low temperature,  
423 considering the thermal stability of the dye and its speciation.



424  
425 Figure 5- TEM images for i) CA-precSap-120 and ii) CA-precMt-120.

426

427 *4.6 Time-resolved fluorescence*

428

429 In previous works, the interaction of clay minerals with anthraquinone dyes has been  
430 observed providing results regarding the stability of the formed systems. [4,6,14,16]. As  
431 described by Fournier, F. *et al.* 2016 [4], the fluorescence property of carminic acid is entirely  
432 related to the environment in which it is inserted. Compared to our previous work, here the  
433 fluorescence lifetime was measured directly on the powder in order to be compared with the  
434 result obtained by the other techniques (NMR, XRD, FTIR). It results that the average



435 lifetime was found to be 0.052 ns while it is about 0.2 ns in water[16]. The fluorescence decay  
436 is well fitted by three components 0.492 ns, 0.107 ns and 0.025 ns where the main one is the  
437 shortest (71.52 %), as shown in Table 2. After co-precipitation on Mt and Sap, the mean  
438 lifetime decreases to 0.035 and 0.012 respectively. However, the long lifetime component  
439 increases from 0.49 ns to ~1 ns. This confirms the interaction between the CA and the  
440 inorganic precursor. However these interactions are weak since we could expect that the  
441 confinement will significantly increase the fluorescence lifetime as previously shown [4,16].  
442 For the both clays, the introduction of HDTMS molecules increases the average lifetime that  
443 is only due to a lengthening of the long component and its yield. This could be assigned to a  
444 hydrophobic environment of the CA. Indeed, it was found that the length of carbon chain of  
445 primary alcohol increases the fluorescence lifetime of CA considering the same protonation  
446 state [54].

447 For the CA@PilSap, we can observe a significant lengthening of the main fluorescent lifetime  
448 (1.089 ns) compared to the CA-precSap-120. The long and average component has yield  
449 about 33 % each. This can be assigned to the presence of penta-coordinated aluminum that  
450 chelates the CA. In that case, the CA is stabilized.

451

452

453

454

455

456

457

458

459

460 Table 2- Fluorescence lifetime ( $\tau_i$ ) and average lifetime ( $\tau_{av}$ )

Samples	$\tau_1$ (ns) / (yield)	$\tau_2$ (ns) / (yield)	$\tau_3$ (ns) / (yied)	$\tau_4$ (ns) / (yied)	$\tau_{(av)}$ (ns)
CA	0.492 (1.29)	0.107 (27.19)	0.025 (71.52)	-	0.053
CA@PilSap	2.447 (34.29)	0.626 (33.47)	0.19 (18.41)	0.043 (13.82)	1.089
CA-precSap-120	0.923 (0.7)	0.204 (0.13)	0.004 (98.75)		0.012
CA-precSap-120-Si	1.542 (4.9)	0.198 (1.34)	0.003 (93.75)		0.081
CA-precMt-120	1.096 (2.57)	0.273 (1.9)	0.002 (95.53)		0.035
CA-precMt-120-Si	1.288 (6.99)	0.279 (3.61)	0.001 (89.4)		0.101

461

462

#### 463 4.7 Desorption tests

464 Desorption tests performed on the samples containing carminic acid showed dye release in  
 465 water, as can be seen in the spectra obtained in solution for CA@Sap, CA-precSap-120 and  
 466 CA-precMt-120, Figure SM2. Maximum released amounts were 47, 65 and 70 mg L<sup>-1</sup>,  
 467 respectively. Aluminium-pillared, CA-precSap-120-Si and CA-precMt-120-Si sample did not  
 468 present any desorption in water or ethanol.

469

#### 470 4.8 Contact surface angle tests

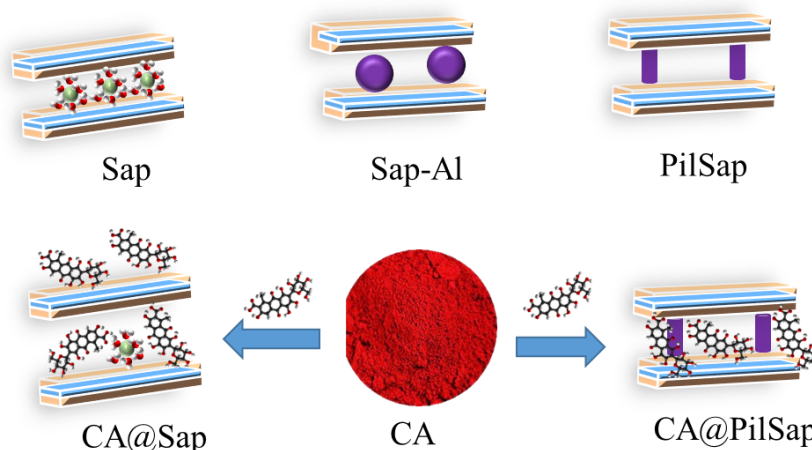
471

472 A contact angle of 133.8 ° was obtained for CA-precSap-120-Si and 130.9 ° for CA-precMt-  
 473 120-Si. Both samples have hydrophobic surfaces with contact angle values higher than 90°.  
 474 Figure SM3 showed the pigment immiscibility in water.

475 4.9 Discussion

476

477 The results showed that the prepared pigments by adsorption presented different  
478 characteristics from those produced via hydrothermal treatment process. This fact is directly  
479 related to the speciation of carminic acid. The synthesis of CA@Sap and CA@PilSap was  
480 realized at pH 2.5 ( $pK_{a1} = 2.8$ ). At that pH, the dye is mainly in its neutral form interacting  
481 directly or indirectly through water bridges with the exchangeable cations in the interlayer  
482 space. Moreover, some of the adsorbed CA molecules may involve hydrogen-bonds between  
483 the CO function and the water molecules that are present in the clay structure [55]. In the  
484 CA@PilSap sample, chelation occurs between the aluminium pillars and the dye promoting  
485 dye stabilization. as showed in the FTIR and  $^{27}\text{Al}$  NMR results (Figure 6).

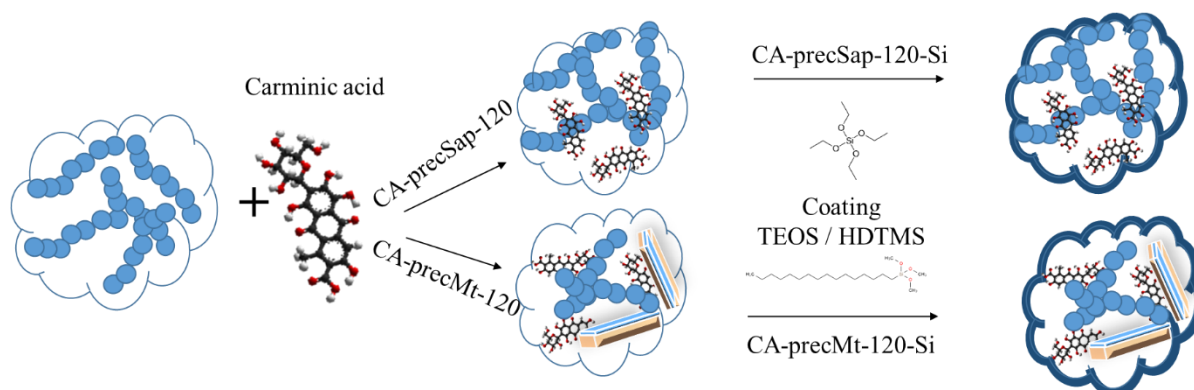


486

487 Figure 6. Scheme for formation of the CA@Sap and CA@PilSap pigments.

488 Although the clay minerals were not obtained, the presence of metal oxides in the hydrogel  
489 can promote the same kind of interactions with the dye, as observed in CA@PilSap (Figure  
490 7). However, an important point should be underlined. The synthesis of the clay minerals was  
491 at pH values between 4 and 5 and under these conditions part of the carminic acid molecules

492 are in their mono-anionic forms ( $pK_{a2} = 5.4$ ), which explain the partial desorption of the  
493 samples without coating, when in contact with water [4].



494

495 Figure 7- Scheme for the formation of coprecipitated and coated TEOS/HDTMS pigments

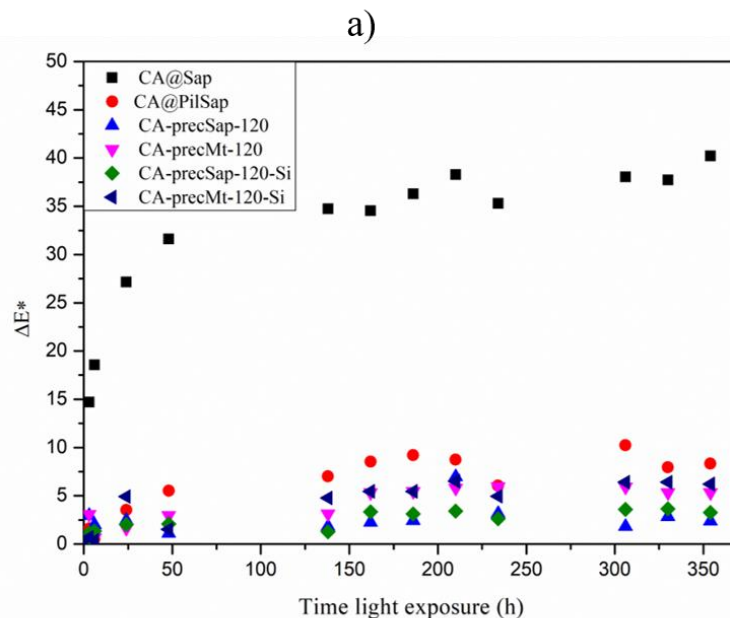
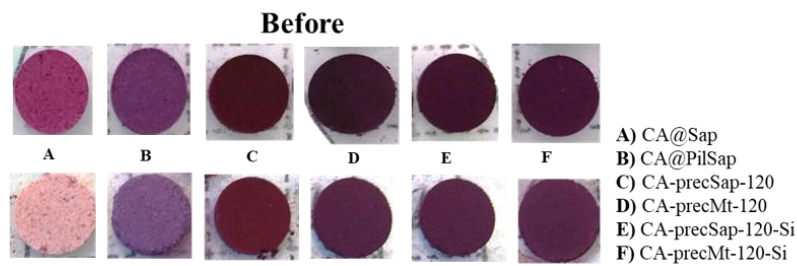
#### 496 4.10 Color and hue variation of the hybrid pigments and photostability tests

497 UV-Vis spectrum of carminic acid showed a wide absorption range centered at 476 nm in the  
498 visible region attributed to  $n \rightarrow \pi^*$  transitions related to the chromaticity in the dye molecule  
499 [39]. Figure SM4i showed significant blue shift (530 nm) in the Sap and PilSap samples,  
500 compared to the one observed in isolated carminic acid. It has been suggested that the p-  
501 electrons of the dye can interact with the hybridized orbitals of the oxygen atoms at the  
502 surface of the clay, leading to a stabilization of the  $\pi^*$  orbitals and destabilization of the  $\pi$ -  
503 orbitals, giving rise to a red shift of the absorption band of the adsorbed CA molecules  
504 [56,57].

505 CA@PilSap hybrid showed a slight decrease in the intensity and the band shifted to 541 nm.  
506 In contrast, CA@Sap showed the disappearance of the carminic acid band after irradiation  
507 (Figure 8a). The hybrid pigments prepared by coprecipitation presented similar profiles. Both  
508 spectra exhibited a wide band centered at 516 nm for CA-precSap-120 and CA-precSap-120-  
509 Si and 522 nm for CA-precMt-120 and CA-precMt-120-Si (Figure SM4iii). The differences  
510 observed for solid pigments after light exposure is probably due to the degradation/fading of  
511 the dye. Furthermore, the low photostability of CA@Sap compared to CA@PilSap suggested

512 weak interactions between the dye and the inorganic matrix as also attested by the release of  
 513 the dye in the desorption experiments [6,16].

514 Photostability is an important parameter to evaluate pigments. Thus, the prepared pigments  
 515 were evaluated face to visible light exposure with illuminance capacity of 66 klx for 354 h.  
 516 These conditions are equivalent to approximately 39 years under normal illumination  
 517 exposure for oil paintings in a museum (200 Lux; 10 h of light exposure per day; 6 days per  
 518 week; 50 weeks per year) [6,19,58,59]. The measurement over CIE  $L^*$ ,  $a^*$  and  $b^*$  scales notice  
 519 a quantitative change over the pigments.  $\Delta E^*$  variation values are due to the change of  
 520 pigment structure after light exposure [6]. Color and hue variation of the hybrids obtained  
 521 from these parameters for both unaged and aged pigments are presented in Figure 8-ab.



b)

522

523 Figure 8- a) Solid pigments and b) color differences ( $\Delta E^*$ ) between samples before and after  
524 light exposure for 354 h with 66 klx of illumination intensity.

525

526  $\Delta E^*$  values provide information on pigment stability once the higher values demonstrate  
527 lower stability [60]. Thus, from the data the dye presented higher values of  $\Delta E^*$  (more than  
528 30) when adsorbed on saponite. In contrast, all hybrid pigments formed from pillarization or  
529 coprecipitation presented high stability with  $\Delta E^*$  values lower than 10. Al-pillared based  
530 pigments were more stable than other polycations (e.g., Ti-pillared) [6]. Moreover,  $\Delta E^*$   
531 values for Al-pillared saponite were lower than ones for Al-pillared montmorillonite pigments  
532 ( $\Delta E^* \sim 14$ ) [6,16].

533 Hybrid pigments formed from coprecipitation presented high stability with  $\Delta E^*$  values lower  
534 than 7. In the first 138 h of exposure, both samples (CA-precSap-120-Si and CA-precMt-120-  
535 Si) presented lower  $\Delta E^*$  values than those obtained for uncoated samples. These results  
536 suggested a higher stability for the coated samples. Indeed, coating the surface of the pigment  
537 disturbs the reactions with oxygen. [6,61]. TEOS / HDTMS coating acts as an inhibitor in the  
538 formation of the radicals by the formation of a protective layer. The similar effect can also  
539 occur for the dye molecules intercalated in the interlayer space of clay mineral.

540

## 541 **5. Conclusions**

542

543 Preparation of hybrid pigments through different methodologies resulted in new solids with  
544 improved properties compared with raw materials. XRD results suggested the intercalation of  
545 CA in the interlayer space of saponite in CA@SAP samples. CA desorption in both  
546 CA@PilSap and CA@Sap samples in water or alcohol was not observed. Regarding the  
547 samples produced by hydrothermal synthesis from saponite and montmorillonite precursor

548 gels, the XRD and TEM showed that the clay minerals were not formed, however, it was  
549 possible to observe in CA-precMt-120 micrograph the presence of some layered structures. In  
550 general, the CA adsorption in raw saponite did not generate stable hybrid pigments. In  
551 contrast, pillarization provided stronger interactions between the inorganic matrix and the dye,  
552 and resulted in more stable pigments. The "encapsulation" of the dye in saponite and  
553 montmorillonite precursor hydrogels seemed to be effective for the photostability concern,  
554 generating pigments highly stable to light exposure. Moreover, pigment coating was effective,  
555 also providing an increase in the stability of the prepared pigments.

556

### 557 **Acknowledgements**

558

559 We acknowledge the financial support from the CAPES/COFEBUB (Project n° 835/15). The  
560 authors thank the Île-de-France region and CNRS for funding.

561

### 562 **References**

- 563 [1] Donkin RA. The Insect Dyes of Western and West-Central Asia.  
564 *Anthropos* 1977;72:847–80.
- 565 [2] Rasmussen SA, Kongstad KT, Khorsand-Jamal P, Kannangara RM,  
566 Nafisi M, Van Dam A, et al. On the biosynthetic origin of carminic  
567 acid. *Insect Biochem Mol Biol* 2018;96:51–61.  
568 doi:10.1016/j.ibmb.2018.03.002.
- 569 [3] Dapson RW. The history, chemistry and modes of action of carmine  
570 and related dyes. *Biotech Histochem* 2007;82:173–87.  
571 doi:10.1080/10520290701704188.
- 572 [4] Fournier F, de Viguerie L, Balme S, Janot JM, Walter P, Jaber M.

- 573 Physico-chemical characterization of lake pigments based on  
574 montmorillonite and carminic acid. *Appl Clay Sci* 2016;130:12–7.  
575 doi:10.1016/j.clay.2016.01.046.
- 576 [5] Rader Bowers LM, Schmidtke Sobeck SJ. Impact of medium and  
577 ambient environment on the photodegradation of carmine in  
578 solution and paints. *Dye Pigment* 2016;127:18–24.  
579 doi:10.1016/j.dyepig.2015.12.012.
- 580 [6] Trigueiro P, Pereira FAR, Guillermin D, Rigaud B, Balme S, Janot  
581 J-M, et al. When anthraquinone dyes meet pillared montmorillonite:  
582 Stability or fading upon exposure to light? *Dye Pigment*  
583 2018;159:384–94. doi:10.1016/j.dyepig.2018.06.046.
- 584 [7] Chen H, Zhang Z, Zhuang G, Jiang R. A new method to prepare  
585 ‘Maya red’ pigment from sepiolite and Basic red 46. *Appl Clay Sci*  
586 2019;174:38–46. doi:10.1016/j.clay.2019.03.023.
- 587 [8] Zhang Y, Zhang J, Wang A. From Maya blue to biomimetic  
588 pigments: Durable biomimetic pigments with self-cleaning  
589 property. *J Mater Chem A* 2016;4:901–7. doi:10.1039/c5ta09300g.
- 590 [9] Sánchez del Río M, Martinetto P, Reyes-Valerio C, Dooryhée E,  
591 Suárez M. Synthesis and acid resistance of Maya blue pigment.  
592 *Archaeometry* 2006;48:115–30. doi:10.1111/j.1475-  
593 4754.2006.00246.x.
- 594 [10] Brigatti MF, Galán E, Theng BKG. Structure and Mineralogy of  
595 Clay Minerals. vol. 5. 2013. doi:10.1016/B978-0-08-098258-  
596 8.00002-X.
- 597 [11] Kausar A, Iqbal M, Javed A, Aftab K, Nazli Z i. H, Bhatti HN, et al.



- 598 Dyes adsorption using clay and modified clay: A review. *J Mol Liq*  
599 2018;256:395–407. doi:10.1016/j.molliq.2018.02.034.
- 600 [12] Espantaleón AG, Nieto JA, Fernández M, Marsal A. Use of  
601 activated clays in the removal of dyes and surfactants from tannery  
602 waste waters. *Appl Clay Sci* 2003;24:105–10. doi:10.1016/S0169-  
603 1317(03)00153-4.
- 604 [13] Adeyemo AA, Adeoye IO, Bello OS. Adsorption of dyes using  
605 different types of clay: a review. *Appl Water Sci* 2017;7:543–68.  
606 doi:10.1007/s13201-015-0322-y.
- 607 [14] Tangaraj V, Janot JM, Jaber M, Bechelany M, Balme S. Adsorption  
608 and photophysical properties of fluorescent dyes over  
609 montmorillonite and saponite modified by surfactant. *Chemosphere*  
610 2017;184:1355–61. doi:10.1016/j.chemosphere.2017.06.126.
- 611 [15] Clécio L, Lima B, Castro-silva F, Silva-filho EC. Saponite-  
612 anthocyanin pigments: slipping between the sheets. *Microporous*  
613 *Mesoporous Mater* 2020;110148.  
614 doi:10.1016/j.micromeso.2020.110148.
- 615 [16] Guillermin D, Debroise T, Trigueiro P, de Viguierie L, Rigaud B,  
616 Morlet-Savary F, et al. New pigments based on carminic acid and  
617 smectites: A molecular investigation. *Dye Pigment* 2019;160:971–  
618 82. doi:10.1016/j.dyepig.2018.07.021.
- 619 [17] Silva GTM, Silva CP, Gehlen MH, Oake J, Bohne C, Quina FH.  
620 Organic/inorganic hybrid pigments from flavylum cations and  
621 palygorskite. *Appl Clay Sci* 2018;162:478–86.  
622 doi:10.1016/j.clay.2018.07.002.

- 623 [18] Tian G, Wang W, Mu B, Wang Q, Wang A. Cost-efficient, vivid  
624 and stable red hybrid pigments derived from naturally available  
625 sepiolite and halloysite. *Ceram Int* 2017;43:1862–9.  
626 doi:10.1016/j.ceramint.2016.10.145.
- 627 [19] Zhuang G, Rodrigues F, Zhang Z, Fonseca MG, Walter P, Jaber M.  
628 Dressing protective clothing: stabilizing alizarin/halloysite hybrid  
629 pigment and beyond. *Dye Pigment* 2019;166:32–41.  
630 doi:10.1016/j.dyepig.2019.03.006.
- 631 [20] Teepakakorn AP, Bureekaew S, Ogawa M. Adsorption-Induced  
632 Dye Stability of Cationic Dyes on Clay Nanosheets. *Langmuir*  
633 2018;34:14069–75. doi:10.1021/acs.langmuir.8b02978.
- 634 [21] Saavedra-Labastida E, Díaz-Nava MC, Illescas J, Muro C.  
635 Comparison of the Removal of an Anionic Dye from Aqueous  
636 Solutions by Adsorption with Organically Modified Clays and their  
637 Composites. *Water Air Soil Pollut* 2019;230. doi:10.1007/s11270-  
638 019-4131-z.
- 639 [22] Ngulube T, Gumbo JR, Masindi V, Maity A. An update on  
640 synthetic dyes adsorption onto clay based minerals: A state-of-art  
641 review. *J Environ Manage* 2017;191:35–57.  
642 doi:10.1016/j.jenvman.2016.12.031.
- 643 [23] Bertuoli PT, Piazza D, Scienza LC, Zattera AJ. Preparation and  
644 characterization of montmorillonite modified with 3-  
645 aminopropyltriethoxysilane. *Appl Clay Sci* 2014;87:46–51.  
646 doi:10.1016/j.clay.2013.11.020.
- 647 [24] Švara Fabjan E, Otoničar M, Gaberšček M, Sever Škapin A. Surface

648 protection of an organic pigment based on a modification using a  
649 mixed-micelle system. *Dye Pigment* 2016;127:100–9.  
650 doi:10.1016/j.dyepig.2015.12.016.

651 [25] A.R. Pereira F, S. Sousa K, R.S. Cavalcanti G, B. França D, N.F.  
652 Queiroga L, Santos I, et al. Green biosorbents based on chitosan-  
653 montmorillonite beads for anionic dye removal. vol. 5. 2017.  
654 doi:10.1016/j.jece.2017.06.032.

655 [26] Brito DF, Da Silva Filho EC, Fonseca MG, Jaber M. Organophilic  
656 bentonites obtained by microwave heating as adsorbents for anionic  
657 dyes. *J Environ Chem Eng* 2018;6:7080–90.  
658 doi:10.1016/j.jece.2018.11.006.

659 [27] Bertella F, Pergher SBC. Pillaring of bentonite clay with Al and Co.  
660 *Microporous Mesoporous Mater* 2015;201:116–23.  
661 doi:10.1016/j.micromeso.2014.09.013.

662 [28] Queiroga LNF, Pereira MBB, Silva LS, Silva Filho EC, Santos  
663 IMG, Fonseca MG, et al. Microwave bentonite silylation for dye  
664 removal: Influence of the solvent. *Appl Clay Sci* 2019;168:478–87.  
665 doi:10.1016/j.clay.2018.11.027.

666 [29] Dong J, Wang Q, Zhang Y, Zhu Z, Xu X, Zhang J, et al. Colorful  
667 superamphiphobic coatings with low sliding angles and high  
668 durability based on natural nanorods. *ACS Appl Mater Interfaces*  
669 2017;9:1941–52. doi:10.1021/acsami.6b13539.

670 [30] Jaber M, Brendlé J. Influence du milieu de synthèse sur la  
671 cristallisation de saponite: proposition de mécanisme réactionnel en  
672 milieux acide et basique. vol. 8. *Comptes*. 2005.

- 673 doi:10.1016/j.crci.2004.10.025.
- 674 [31] Bergaoui L, Lambert JF, Suquet H, Che M. CuII on Al13-pillared  
675 saponites: Macroscopic adsorption measurements and EPR spectra.  
676 J Phys Chem 1995;99:2155–61. doi:10.1021/j100007a054.
- 677 [32] Latthe SS, Hirashima H, Rao AV. TEOS based water repellent  
678 silica films obtained by a co-precursor sol-gel method. Smart Mater  
679 Struct 2009;18. doi:10.1088/0964-1726/18/9/095017.
- 680 [33] Bisio C, Gatti G, Boccaleri E, Marchese L, Superti GB, Pastore HO,  
681 et al. Understanding physico-chemical properties of saponite  
682 synthetic clays. Microporous Mesoporous Mater 2008;107:90–101.  
683 doi:10.1016/j.micromeso.2007.05.038.
- 684 [34] Jaber M, Miéché-Brendlé J. Influence du milieu de synthèse sur la  
685 cristallisation de saponite: Proposition de mécanisme réactionnel en  
686 milieux acide et basique. Comptes Rendus Chim 2005;8:229–34.  
687 doi:10.1016/j.crci.2004.10.025.
- 688 [35] Prieto O, Vicente MA, Angel Bañares-Muñoz M. Study of the  
689 Porous Solids Obtained by Acid Treatment of a High Surface Area  
690 Saponite. vol. 6. 1999. doi:10.1023/A:1009657312123.
- 691 [36] Tangaraj V, Janot J-M, Jaber M, Bechelany M, Balme S.  
692 Adsorption and photophysical properties of fluorescent dyes over  
693 montmorillonite and saponite modified by surfactant. Chemosphere  
694 2017;184:1355–61. doi:10.1016/j.chemosphere.2017.06.126.
- 695 [37] Bergaya F, Theng BKG, Lagaly G. Pillared Clays and Clay  
696 Minerals. vol. 5. 2nd ed. Elsevier Ltd.; 2013. doi:10.1016/B978-0-  
697 08-098258-8.09992-2.

- 698 [38] Figueras F. Pillared Clays as Catalysts. *Catal Rev* 1988;30:457–99.  
699 doi:10.1080/01614948808080811.
- 700 [39] Munir S, Shah SM, Hussain H, Siddiq M. Adsorption of porphyrin  
701 and carminic acid on TiO<sub>2</sub> nanoparticles: A photo-active nano-  
702 hybrid material for hybrid bulk heterojunction solar cells. *J*  
703 *Photochem Photobiol B Biol* 2015;153:397–404.  
704 doi:10.1016/j.jphotobiol.2015.10.029.
- 705 [40] Pérez E, Ibarra IA, Guzmán A, Lima E. Hybrid pigments resulting  
706 from several guest dyes onto  $\gamma$ -alumina host: A spectroscopic  
707 analysis. *Spectrochim Acta - Part A Mol Biomol Spectrosc*  
708 2017;172:174–81. doi:10.1016/j.saa.2016.04.017.
- 709 [41] Tao Q, Fang Y, Li T, Zhang D, Chen M, Ji S, et al. Silylation of  
710 saponite with 3-aminopropyltriethoxysilane. *Appl Clay Sci*  
711 2016;132–133:133–9. doi:10.1016/j.clay.2016.05.026.
- 712 [42] S. Petit and J. Madejova. *Fourier Transform Infrared Spectroscopy*.  
713 vol. 5. 2nd ed. Elsevier Ltd.; 2013. doi:10.1007/978-3-642-74065-  
714 7\_7.
- 715 [43] Wang W, Kang Y, Wang A. Synthesis, characterization and  
716 swelling properties of guar gum-g-poly(sodium acrylate-co-  
717 styrene)/muscovite superabsorbent composites. *Sci Technol Adv*  
718 *Mater* 2010;11:25006. doi:10.1088/1468-6996/11/2/025006.
- 719 [44] Földvári M. *Handbook of the thermogravimetric system of minerals*  
720 *and its use in geological practice*. vol. 56. 2011.  
721 doi:10.1556/CEuGeol.56.2013.4.6.
- 722 [45] Marzec A, Szadkowski B, Rogowski J, Maniukiewicz W,

- 723 Kozanecki M, Moszyński D, et al. Characterization and properties  
724 of new color-tunable hybrid pigments based on layered double  
725 hydroxides (LDH) and 1,2-dihydroxyanthraquinone dye. *J Ind Eng*  
726 *Chem* 2019;70:427–38. doi:10.1016/j.jiec.2018.11.005.
- 727 [46] Gil A, Korili SA, Trujillano R, Vicente MA. A review on  
728 characterization of pillared clays by specific techniques. *Appl Clay*  
729 *Sci* 2011;53:97–105. doi:10.1016/j.clay.2010.09.018.
- 730 [47] Bergaoui L, Mrad I, Lambert J-F, Ghorbel A. A Comparative Study  
731 of the Acidity toward the Aqueous Phase and Adsorptive Properties  
732 of Al<sub>13</sub>-Pillared Montmorillonite and Al<sub>13</sub>-Pillared Saponite. *J*  
733 *Phys Chem B* 2002;103:2897–902. doi:10.1021/jp984011e.
- 734 [48] Furrer G, Ludwig C, Schindler PW. On the chemistry of the Keggin  
735 Al<sub>13</sub> polymer. I. Acid-base properties. *J Colloid Interface Sci*  
736 1992;149:56–67. doi:10.1016/0021-9797(92)90391-X.
- 737 [49] Kooli F, Jones W. Systematic Comparison of a Saponite Clay  
738 Pillared with Al and Zr Metal Oxides. *Chem Mater* 1997;9:2913–  
739 20. doi:10.1021/cm970254s.
- 740 [50] Pérez-Ramírez E, Lima E, Guzmán A. Natural betalains supported  
741 on  $\gamma$ -alumina: A wide family of stable pigments. *Dye Pigment*  
742 2015;120:161–8. doi:10.1016/j.dyepig.2015.03.040.
- 743 [51] Pérez E, Ibarra IA, Guzmán A, Lima E. Hybrid pigments resulting  
744 from several guest dyes onto  $\gamma$ -alumina host: A spectroscopic  
745 analysis. *Spectrochim Acta - Part A Mol Biomol Spectrosc*  
746 2017;172:174–81. doi:10.1016/j.saa.2016.04.017.
- 747 [52] Zhang D, Zhou CH, Lin CX, Tong DS, Yu WH. Synthesis of clay

748 minerals. Appl Clay Sci 2010;50:1–11.  
749 doi:10.1016/j.clay.2010.06.019.

750 [53] Gao K, Chang Q, Wang B, Zhou N, Qing T. Synthetic magnesium  
751 silicate hydroxide nanoparticles coated with carbonaceous shell in  
752 subcritical water condition. Appl Surf Sci 2018;450:312–7.  
753 doi:10.1016/j.apsusc.2018.04.139.

754 [54] Rasimas JP, Blanchard GJ. A study of the fluorescence and  
755 reorientation dynamics of carminic acid in primary alcohols. J Phys  
756 Chem 1995;99:11333–8. doi:10.1021/j100029a006.

757 [55] Akyuz S, Akyuz T. FT-IR and FT-Raman spectroscopic studies of  
758 adsorption of isoniazid by montmorillonite and saponite. Vib  
759 Spectrosc 2008;48:229–32. doi:10.1016/j.vibspec.2008.02.019.

760 [56] Schoonheydt R, Johnston C. Surface and interface chemistry of clay  
761 minerals. vol. 1. 2nd ed. Elsevier Ltd.; 2013. doi:10.1016/S1572-  
762 4352(05)01003-2.

763 [57] Gonçalves JLS, Valandro SR, Poli AL, Schmitt CC. Influence of  
764 clay minerals on curcumin properties: Stability and singlet oxygen  
765 generation. J Mol Struct 2017;1143:1–7.  
766 doi:10.1016/j.molstruc.2017.04.073.

767 [58] Zhuang G, Jaber M, Rodrigues F, Rigaud B, Walter P, Zhang Z. A  
768 new durable pigment with hydrophobic surface based on natural  
769 nanotubes and indigo: Interactions and stability. J Colloid Interface  
770 Sci 2019;552:204–17. doi:10.1016/j.jcis.2019.04.072.

771 [59] De Queiroga LNF, França DB, Rodrigues F, Santos IMG, Fonseca  
772 MG, Jaber M. Functionalized bentonites for dye adsorption:

773 Depollution and production of new pigments. *J Environ Chem Eng*  
774 2019;7:103333. doi:10.1016/j.jece.2019.103333.

775 [60] Kokalj D, Zlatić E, Cigić B, Vidrih R. Postharvest light-emitting  
776 diode irradiation of sweet cherries (*Prunus avium* L.) promotes  
777 accumulation of anthocyanins. *Postharvest Biol Technol*  
778 2019;148:192–9. doi:10.1016/j.postharvbio.2018.11.011.

779 [61] Lencione D, Gehlen MH, Trujillo LN, Leitao RCF, Albuquerque  
780 RQ. The spatial distribution of the photostability of thionine in  
781 zeolite L nanochannels investigated by Photobleaching Lifetime  
782 Imaging Microscopy. *Photochem Photobiol Sci* 2016;15:398–404.  
783 doi:10.1039/c5pp00418g.

784